Metal-Enhanced Upconversion Luminescence Tunable through Metal Nanoparticle–Nanophosphor Separation

Marjan Saboktakin,[†] Xingchen Ye,[‡] Soong Ju Oh,[§] Sung-Hoon Hong,[†] Aaron T. Fafarman,[†] Uday K. Chettiar,[†] Nader Engheta,[†,⊥,∥] Christopher B. Murray,[‡,§] and Cherie R. Kagan[†,‡,§,*]

[†]Department of Electrical and Systems Engineering, [‡]Department of Chemistry, [§]Department of Materials Science and Engineering, [⊥]Department of Bioengineering, and [∥]Department of Physics and Astronomy, University of Pennsylvania, Philadelphia, Pennsylvania 19104, United States

ABSTRACT

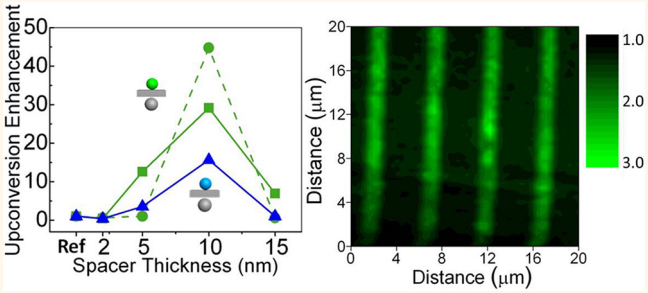

We have demonstrated amplification of luminescence in upconversion nanophosphors (UCNPs) of hexagonal phase $NaYF_4$ (β-$NaYF_4$) doped with the lanthanide dopants Yb^{3+}, Er^{3+} or Yb^{3+}, Tm^{3+} by close proximity to metal nanoparticles (NPs). We present a configuration in which close-packed monolayers of UCNPs are separated from a dense multilayer of metal NPs (Au or Ag) by a nanometer-scale oxide grown by atomic layer deposition. Luminescence enhancements were found to be dependent on the thickness of the oxide spacer layer and the type of metal NP with enhancements of up to 5.2-fold proximal to Au NPs and of up to 45-fold proximal to Ag NPs. Concomitant shortening of the UCNP luminescence decay time and rise time is indicative of the enhancement of the UCNP luminescence induced by resonant plasmonic coupling and nonresonant near-field enhancement from the metal NP layer, respectively.

KEYWORDS: upconversion · nanophosphor · plasmonically enhanced emission · metal-enhanced absorption · lanthanide · atomic layer deposition · nanoimprint lithography

The ability to control and fine-tune the spectral properties of upconversion nanocrystalline phosphors (UCNPs), which can emit light at shorter wavelengths than the excitation source, has been of considerable interest in recent years due to their applications in biomedical imaging,[1] solar cells,[2−4] lasers,[5] lighting, and display technologies.[6] Among upconverting materials, the β-$NaYF_4$ host lattice doped with lanthanide combinations of Yb^{3+}, Er^{3+} or Yb^{3+}, Tm^{3+} has been shown to be the most efficient UCNPs.[7] The crystal field and phonon structure of $NaYF_4$ strongly affect the efficiency of energy transfer between dopants that gives rise to upconversion.[8] However, the efficiency of upconversion in these materials remains low[9] due to the small absorption cross sections arising from formally forbidden f-level atomic transitions of the dopants, prompting a need for methods of enhancing their luminescence.

Placing UCNPs in close proximity to plasmonic metal surfaces or random distributions of metal nanoparticles (NPs) such as gold (Au), silver (Ag), or aluminum (Al) has shown promising enhancements in upconversion efficiency.[10−13] Close proximity of metal NPs to UCNPs can cause luminescence enhancement in UCNPs by influencing both absorption in the near-infrared and emission at shorter wavelengths in the visible. When light impinges on a metal NP, it interacts with the free electrons of the metal, causing charge and current oscillations within the skin depth of the metal surface. At wavelengths resonant with the metal NP plasmon frequency, this interaction results in local electric field strengths that are much higher than that of the incident electromagnetic field. Metal NPs can influence the emission process if their resonant wavelength overlaps with the emission frequency of the UCNPs, similar to the common mechanism of emission enhancement in other fluorophors.[14,15] However, even at excitation wavelengths off-resonance with the metal NP plasmon frequency, these oscillations create an electromagnetic

* Address correspondence to kagan@seas.upenn.edu.

Received for review June 4, 2012 and accepted September 1, 2012.

Published online September 01, 2012
10.1021/nn302466r

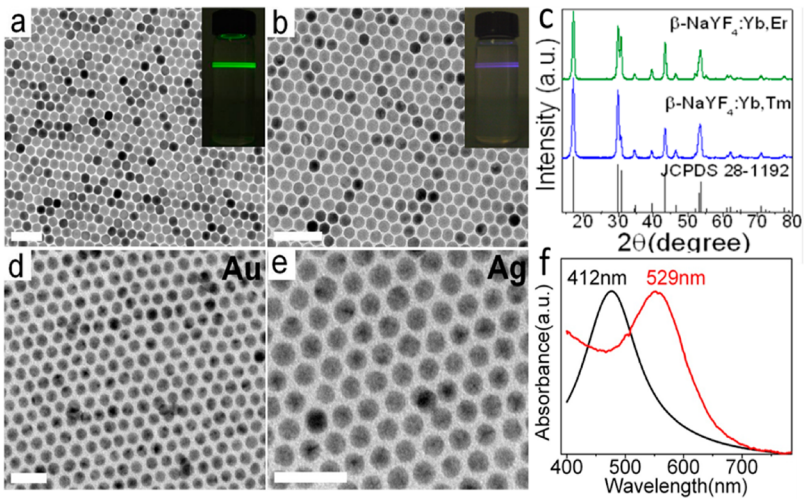

Figure 1. TEM images of (a) $NaYF_4$:Yb, Er and (b) $NaYF_4$:Yb, Tm UCNPs. Insets are photographs showing the upconversion luminescence from hexane solution of UCNPs under 980 nm laser excitation. (c) Powder X-ray diffraction pattern of the hexagonal phase UCNPs (β-NaYF4). TEM images of (d) Au and (e) Ag NPs and (f) absorption spectra of Au (red curve) and Ag (black curve) NPs dispersed in hexane, normalized to their plasmonic peaks. Scale bars: (a) 100 nm, (b) 100 nm, (d) 20 nm, (e) 20 nm.

field near the surface of the metal NP that strengthens the surrounding field acting on UCNPs. Nonresonant absorption enhancement of near-infrared excitations in UCNPs has been proposed to contribute to the observed upconversion enhancement in UCNPs.[16] Enhanced fields result in higher emission rates in UCNPs, contributing to considerable enhancement of emission intensity in UCNPs in the vicinity of metal NPs.[17]

These metal-induced electromagnetic fields depend strongly on the shape, size, and composition of the metal nanostructures. Various UCNP-metal geometric configurations have been made recently; nanoscale fabrication techniques have been used to engineer plasmonic properties that could achieve emission enhancement factors as high as 4.8.[16] The fabrication methods include electrochemical deposition,[18,19] electron beam lithography,[20−22] and nanosphere lithography.[23] However, the fabrication processes are complex, and NP assembly methods that apply to large areas with good control and selectivity have not been reported. To interrogate the physics of metal-enhanced upconversion, studies have been made on a single UCNP near a metal surface, and while these studies are extremely valuable, the configuration does not usually lend itself to use in many applications.[16,24] Therefore, there is a need for developing more consistent, reproducible, large surface area structures and robust assembly methods.

In this paper, we describe a simple method to fabricate a well-defined multilayered structure composed of monodisperse metal NPs and UCNPs controlled in their separation at the nanometer scale by atomic layer deposition of an intervening Al_2O_3 layer. We use this geometry to macroscopically study the role of the spacer layer thickness on the enhancement process through steady-state photoluminescence (PL) measurements and investigate the nature of the enhancement by time-resolved PL rise and decay time experiments. The aforementioned structures allow us to study the efficiency of upconversion in UCNPs with energies of emission in the blue, green, and red of the visible spectrum in combination with Au or Ag NPs. We show the enhancement of upconverted luminescence depends strongly on both the distance between UCNP and metal NP layers and the choice of metal, with enhancements of up to 45-fold observed using Ag NCs. Lifetime measurements corroborate the measurements of luminescence yield, with the shortest emission rise and decay times corresponding with the maximum emission enhancement. Electromagnetic simulations suggest nonresonant enhancement of near-infrared excitation and resonant plasmonic enhancement of visible emission give rise to the measured decrease in rise and decay times and enhancement of upconverted luminescence in these low-efficiency emitting UCNPs in proximity to metal NPs.

RESULTS AND DISCUSSION

Here, we have taken advantage of a recently developed synthetic route that produces β-$NaYF_4$ nanocrystals while suppressing the formation of the less efficient α-$NaYF_4$ phase.[25−28] The UCNPs are spherical in shape and monodisperse in size (standard deviation $\sigma \approx 5\%$), as seen in transmission electron microscopy (TEM) for Yb^{3+}, Er^{3+} (Figure 1a) and Yb^{3+}, Tm^{3+} (Figure 1b) doped $NaYF_4$. Figure 1c shows the X-ray diffraction patterns of the Yb^{3+}, Er^{3+} and Yb^{3+}, Tm^{3+} doped $NaYF_4$ UCNPs, confirming that they are of pure hexagonal phase. This crystal host doped with combinations of rare earth elements Yb^{3+}, Er^{3+} or Yb^{3+}, Tm^{3+} has provided us an opportunity to study upconversion

luminescence in the green and red regions of the spectrum (centered at 540 and 650 nm, respectively) in $NaYF_4$ codoped with Yb^{3+}, Er^{3+} and in the blue region of the spectrum (centered at 450 and 475 nm) in $NaYF_4$ codoped with Yb^{3+}, Tm^{3+}. The emission of the UCNPs is shown in the insets in Figure 1a, b and the spectra in Figure S1a, b when illuminated under 980 nm light. Moreover, we have employed an interfacial self-assembly method that allows the formation of close-packed UCNP monolayers over extend areas (millimeter scale).[25,29] The ability to form a continuous monolayer of UCNPs using particles that are monodisperse both in phase and in size has given us a great advantage over previously attempted configurations to achieve high luminescence enhancements and consistent results from sample to sample, allowing us to probe metal-induced enhancement of upconversion.

To enhance the emission of these UCNPs, we have prepared spherical Au and Ag NPs, 5 nm in diameter with standard deviation of $\sigma \approx 5\%$, as shown in TEM micrographs (Figure 1d, e). The plasmonic peak for dispersions of Au NPs is at 550 nm, and that for dispersions of Ag NPs is at 420 nm (Figure 1f). These plasmonic peaks show considerable spectral overlap with the luminescence peaks of the UCNPs, indicating that a large resonant enhancement of upconversion emission is possible.

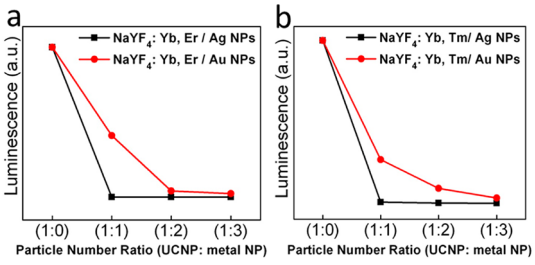

Figure 2. Integrated PL under 980 nm excitation of the (a) 540 nm emission band (510−570 nm) of samples made with mixtures of $NaYF_4$:Yb, Er UCNPs and either Au (red curve) or Ag (black curve) NPs and of the (b) 475 nm emission band (461−490 nm) of samples made with mixtures of $NaYF_4$:Yb, Tm UCNPs and either Au (red curve) or Ag (black curve) NPs with various number ratios of UCNPs:metal NPs.

The existence of the oxide spacer layer is important if any enhancement is to be observed in our proposed structure. To further demonstrate the importance of the dielectric spacer layer, a series of control experiments were performed where UCNPs and metal NPs were mixed in solution form and then were spun on glass substrates. The resulting film consisted of metal NPs and UCNPs in random configurations and distances from each other. Upon illumination of 980 nm laser light (continuous wave), the luminescence intensity of the mixed samples was greatly reduced compared to samples made only with UCNPs (Figure 2). As is evident from Figure 2, the intensity decreases at a lower number fraction of Ag NPs compared to Au NPs. This is consistent with the larger absorption coefficient of Ag *versus* Au NPs. Furthermore, the intensity decreased even more as the volume ratio of metal NPs to UCNPs was increased. In these mixture samples quenching is the dominant process. Introduction of spacer layers as shown in Figure 3a of different thicknesses allows us to find the optimal spacing to maximize the beneficial effects of the metal-induced enhancement while reducing and minimizing the quenching observed in random mixtures.

To fabricate the UCNP−spacer−metal NP structures as shown schematically in Figure 3a, dense Au or Ag NP films were formed on glass substrates by spin-coating. By using solutions with identical concentrations of metal NPs deposited under the same spin-coating conditions, the particle density of the films stays the same from sample to sample. A thin layer of Al_2O_3 was subsequently deposited using atomic layer deposition (ALD). This deposition method provides an accurate thickness of the dielectric spacer on the nanometer scale (Figure S6), which allows precise control over the distance between UCNPs and metal NPs in our structure. After deposition of the oxide layer a slight red shift in the plasmonic peak of the metal NPs is observed, as shown in Figure 3b. The oxide layer therefore also plays an active role in the enhancement of the plasmonic field by affecting the polarization of the metal NPs.[30] Next a large-area monolayer of UCNPs was deposited on top of the oxide layer, as confirmed by scanning

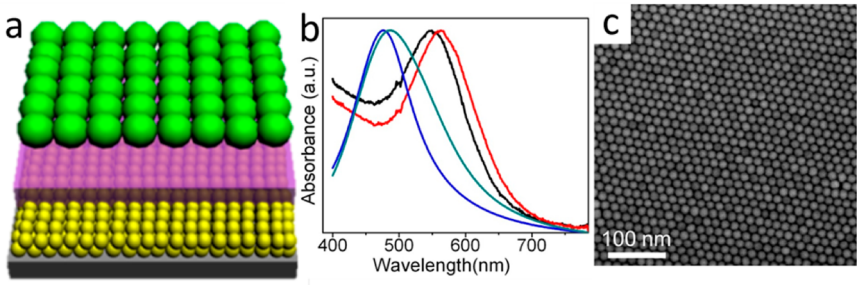

Figure 3. (a) Schematic structure of a spin-cast layer of Au or Ag NPs, a thin Al_2O_3 layer, and a monolayer of UCNPs. (b) Absorption spectra of spin-coated Ag NP films before (blue curve) and after (green curve) deposition of an Al_2O_3 layer and of spin-coated Au NP films before (black curve) and after (red curve) deposition of an Al_2O_3 layer. Each spectrum is normalized by its plasmonic peak absorption. (c) Typical large-area SEM image of a monolayer of UCNPs transferred onto the Al_2O_3 layer-covered metal NP film.

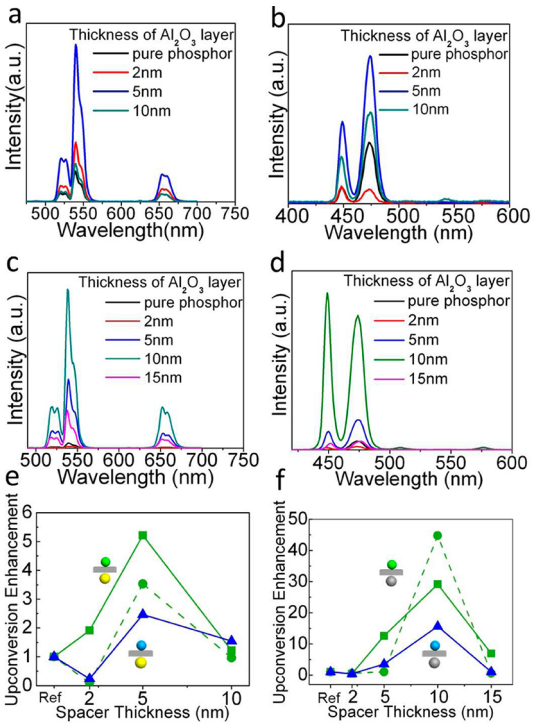

Figure 4. (a–d) Upconversion luminescence spectra of UCNP monolayers transferred onto the Al_2O_3 layer-covered metal NP film under 980 nm excitation. (a) Au NP-Al_2O_3-$NaYF_4$:Yb, Er UCNPs, (b) Au NP-Al_2O_3-$NaYF_4$:Yb, Tm UCNPs, (c) Ag NP-Al_2O_3-$NaYF_4$:Yb, Er UCNPs, (d) Ag NP-Al_2O_3-$NaYF_4$:Yb, Tm UCNPs. Integrated area under the peak as a function of the Al_2O_3 layer thickness normalized to that of the pure UCNP sample for (e) Au NPs and (f) Ag NPs. The green solid lines correspond to the 540 nm emission band (510–570 nm) in $NaYF_4$:Yb, Er. The green dashed lines correspond to the 650 nm emission band (640–680 nm) in $NaYF_4$:Yb, Er. The blue solid lines correspond to the 475 nm emission band (461–490 nm) in $NaYF_4$:Yb, Tm. We have also included the data point corresponding to UCNPs in the absence of metal NPs as a Reference (Ref) in the figure for comparison.

electron microscopy (SEM) for each sample (Figure 3c and Figure S2a, b).

We fabricated the combinations of Au or Ag metal NP layers with either monolayers of $NaYF_4$ UCNPs codoped with Yb^{3+}, Er^{3+} or $NaYF_4$ UCNPs codoped with Yb^{3+}, Tm^{3+} separated by an Al_2O_3 spacer layer. In each of these metal–UCNP combinations, the thickness of the Al_2O_3 spacer layer is tuned from 2 to 15 nm. PL spectra were collected under illumination from a 980 nm continuous wave, 1 W laser. Figure 4a, c show the PL spectra for Yb^{3+}, Er^{3+} doped $NaYF_4$ UCNPs with a characteristic strong emission peak centered at 540 nm in the green resulting from a transition from $S_{3/2}$ to $I_{15/2}$ energy levels and a weaker emission centered at 650 nm in the red resulting from a transition from $F_{9/2}$ to $I_{15/2}$ energy levels (Figure S5). Figure 4b, d show the PL spectra for Yb^{3+}, Tm^{3+} doped $NaYF_4$ UCNPs centered at 450 nm in the blue resulting from a transition from D_2 to F_4 energy levels and 475 nm in the blue resulting from a transition from G_4 to H_6 energy levels. Figure 4a, b show the PL spectra for the combinations of Yb^{3+}, Er^{3+}or Yb^{3+}, Tm^{3+} doped $NaYF_4$ UCNPs spaced from Au NPs, and similarly Figure 4c, d show the PL spectra for the UCNPs spaced from Ag NPs as a function of Al_2O_3 thickness. The emission spectra of the UCNP samples with no metal NP layer are also shown. For samples with a very thin oxide layer, a decrease in emission intensity due to luminescence quenching is observed, similar to the randomly mixed metal NP–UCNP samples (Figure 2). As the oxide layer thickness increases, metal-induced luminescence enhancement of UCNPs is observed. The luminescence enhancement reaches a maximum at a certain thickness, after which the distance between metal NPs and UCNPs becomes too large for metal-induced enhancement, and the emission intensity decreases back to that of the UCNPs alone. The distance at which the largest enhancement occurs is at 5 nm for Au NPs and 10 nm for Ag NPs and is independent of the composition of UCNPs used (Figure 4e, f). There is also a strong dependence of the enhancement on the composition of the metal NPs. As shown in Figure 4e, f, for structures made with Au NPs, we observe enhancement factors of about 5.2 and 3.5 for the 540 and 650 nm peaks of Yb^{3+}, Er^{3+} doped $NaYF_4$ respectively, and much larger enhancement factors of 30 and 45 with Ag NPs for 540 and 650 nm, respectively.

To further demonstrate the contrast between emission of pure UCNPs and metal-enhanced UCNP luminescence, we have used nanoimprint lithography to pattern the metal NP layer into a series of stripes (Figure 5a, b), after which a 5 nm Al_2O_3 spacer layer that is the optimum oxide thickness for Au NPs is deposited. Next, a monolayer of $NaYF_4$ codoped with Yb^{3+}, Er^{3+} was deposited on top of the oxide layer by the interfacial assembly method. A schematic of the final structure is depicted in Figure 5c. Spatially resolved PL measurements demonstrate clearly the spatially selective upconversion enhancement by ~3 times in regions of the UCNP monolayer proximal to the underlying stripe pattern of Au NPs (Figure 5d).

We show that the observed enhancements in upconversion efficiency are due to both plasmonic enhancement of the emission of the UCNPs and metal-induced enhancement of absorption of the excitation pump at 980 nm. In most cases, emission enhancements occur because of factors that reduce the nonradiative decay processes including limiting quenching and lowering the temperature of the environment. However, the fundamental characteristic of metal-induced enhancement at resonant wavelengths is that it directly changes the radiative rate of the UCNP, thereby causing higher emission intensities. We measured the change in the decay rates of the UCNPs by time-resolved PL.

Figure 6a, b show the luminescence decays for $NaYF_4$ codoped with Yb^{3+}, Er^{3+} and Yb^{3+}, Tm^{3+},

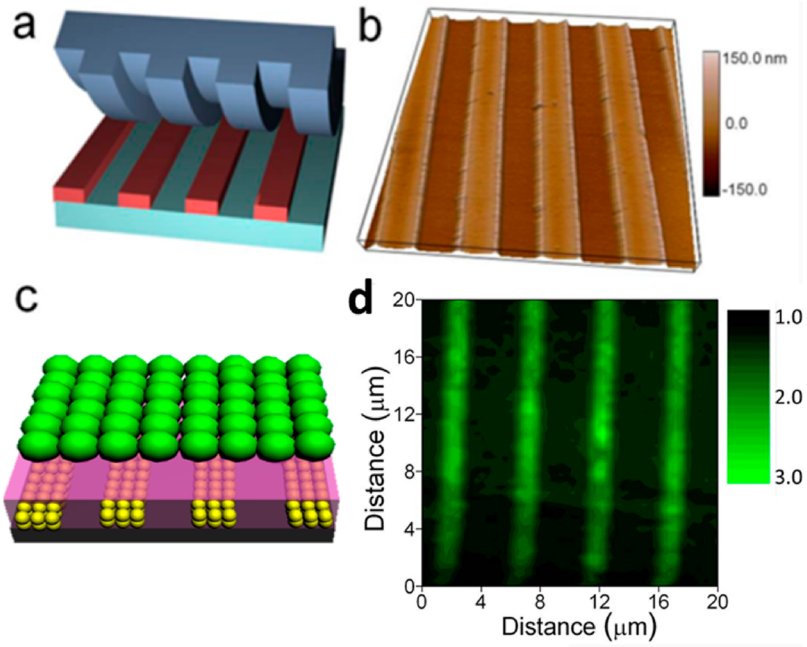

Figure 5. (a) Schematic representation of the nanoimprint lithography process. (b) AFM image of Au NP stripe pattern fabricated by nanoimprint lithography on a glass substrate. Each stripe is about 2 μm in width and 100 nm in height with a periodicity is 5 μm. (c) Schematic illustrating the structure of multilayer films separated by a 5 nm Al_2O_3 layer. (d) Upconversion luminescence mapping of Au NP-Al_2O_3-$NaYF_4$:Yb, Er UCNP films with an Al_2O_3 layer of 5 nm.

respectively, in combination with Au and Ag metal NP layers spaced by oxide layers of different thickness. As the thickness of the oxide spacer layer increases, the UCNP's decay time decreases, reaching a minimum for each of the UCNP compositions at 5 nm for Au NPs and 10 nm for Ag NPs, after which the lifetime increases back to values characteristic of the pure UCNPs (Figure 6c, d). The trend of decay time inversely follows that of the emission enhancement (Figure 4e, f). The decrease in decay times of UCNPs suggests that upconversion enhancement is indeed a metal-induced Purcell effect and is due to the electromagnetic coupling between metal NPs and UCNPs.[31−33] Ag NPs decrease the decay time of UCNPs more significantly than Au NPs (Figure 6c, d).

In addition to the plasmonic increase in the radiative decay rate of UCNPs, metal NPs can cause an enhancement in the absorption of the excitation pump at 980 nm by UCNPs.[16] Measurements reveal the rise time for the 540 nm peak of $NaYF_4$:Yb, Er UCNPs decreases from 0.286 μs for a pure UCNP film to a minimum of 0.236 μs for structures with Au NPs separated by a 5 nm oxide layer and to a minimum of 0.110 μs for structures with Ag NPs separated by a 10 nm oxide layer. For the 475 nm peak of $NaYF_4$:Yb, Tm UCNPs, the rise time decreases from 0.116 μs for a pure UCNP film to a minimum of 0.076 μs for structures with Au NPs and a minimum of 0.035 μs for structures with Ag NPs. Absorption enhancement in UCNPs is caused by nonresonant enhancement of the pump excitation field that results in the faster excitation rate of Yb^{3+}. As a result, the rate of energy transfer from Yb^{3+} to Er^{3+} or Yb^{3+} to Tm^{3+} ions increases (see the energy level scheme, Figure S5), which is in turn manifested by a shorter rise time in the UCNPs.[34] The fact that Ag NPs decrease the rise times and the decay times of the UCNPs more than Au NPs is consistent with the higher luminescence enhancement factors measured in PL measurements.

Amplification of luminescence arises from both absorption enhancement and emission enhancement corresponding with the observed shorter rise and decay times, respectively. To understand the origins of the complex interplay between these factors, the absorption, emission, and overall efficiency enhancement factors as well as the emission decay rate as a function of UCNPs−metal NP distance were simulated using COMSOL Multiphysics software (Figure 7a−d). Absorption enhancement is defined as the ratio of the absorption coefficient of the UCNPs in proximity to metal NPs to the absorption efficiency of UCNPs away from metal NPs. In absorption, nonresonant enhancement of the sensitizing (Yb^{3+}) centers in the UCNPs occurs in proximity to the metal NPs at 980 nm excitation. Since the plasmonic resonances of both Au and Ag NPs are away from the excitation, there is no observable difference in the enhancement of Au and Ag NPs (Figure 7a). The emission enhancement process in our system occurs since Au and Ag NPs are resonant with the UCNP visible emission and the metal NPs change the local photon density of states. It can be shown that the local density of states for photons is related to the Green's function at the emitter.[35] This allowed us to calculate the emission efficiency of UCNPs through classical electromagnetic methods

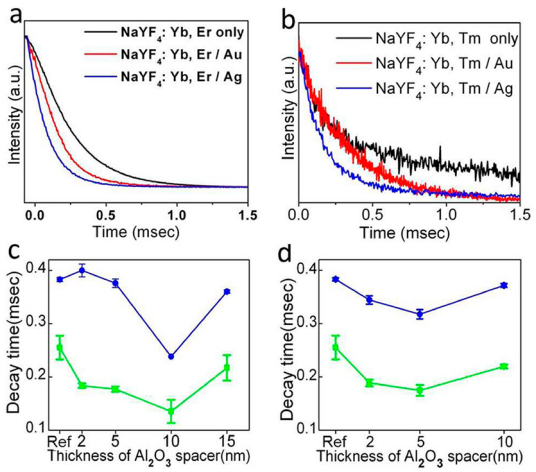

Figure 6. (a) Upconversion luminescence decays monitoring the 540 nm emission under 980 nm excitation of $NaYF_4$:Yb, Er UCNPs separated by a 5 nm thick Al_2O_3 layer from a Au NP film (red curve), $NaYF_4$:Yb, Er UCNPs separated by a 10 nm thick Al_2O_3 layer from a Ag NP film (blue curve), and pure $NaYF_4$:Yb, Er UCNP films (black curve). (b) Upconversion luminescence decays monitoring the 475 nm emission under 980 nm excitation of $NaYF_4$:Yb, Tm UCNPs separated by a 5 nm thick Al_2O_3 layer from a Au NP film (blue curve), $NaYF_4$:Yb, Tm UCNPs separated by a 10 nm thick Al_2O_3 layer from a Ag NP film (red curve), and pure $NaYF_4$:Yb, Tm UCNP films (black curve). (c) Decay times monitoring the 540 nm emission of $NaYF_4$:Yb, Er UCNP films (green curve) and 475 nm emission of $NaYF_4$:Yb, Tm UCNPs (blue curve) under 980 nm excitation separated from Ag NPs as a function of Al_2O_3 spacer layer. (d) Decay times monitoring the 540 nm emission of $NaYF_4$:Yb, Er UCNP films (green curve) and 475 nm emission peak of $NaYF_4$:Yb, Tm UCNPs (blue curve) under 980 nm excitation separated from Au NPs as a function of Al_2O_3 spacer layer. We have also included the data point corresponding to UCNPs in the absence of metal NPs as Reference (Ref) in the figure for comparison.

(Figure 7b). Efficiency enhancement is defined as the ratio of emission efficiency of the UCNPs in proximity to metal NPs in comparison to the emission efficiency of UCNPs away from metal NPs. Simulations show a higher enhancement of UCNPs' efficiency in proximity to Ag NPs compared to Au NPs, consistent with the stronger plasmonic resonance in Ag NPs. Both absorption enhancement and emission efficiency contribute to the overall change in emission enhancement and decay rates of UCNPs (Figure 7c, d). Emission enhancement is calculated as the product of absorption enhancement and emission efficiency and is higher in proximity to Ag NPs compared to Au NPs. The origin of UCNP upconversion enhancement had been speculated previously to be partially due to plasmonic amplification of energy transfer resonant with the second transfer step from $I_{11/2}$ to $F_{7/2}$ (540 nm emission peak) or $I_{13/2}$ to $F_{9/2}$ (650 nm emission peak) between Yb^{3+} and Er^{3+} in $NaYF_4$:Yb^{3+}, Er^{3+} UCNPs.[16] However, since the absorption in UCNPs is a sequential and noncoherent process and the metal NPs have resonances far away from the excitation frequency, plasmonic enhancement to increase energy transfer between atoms in UCNPs appears unlikely. Our simulations reveal these aforementioned speculations are unnecessary, and the observed upconversion enhancement and changes in rise and decay times may be accounted for by nonresonant enhancement in absorption at 980 nm and resonant enhancement in emission at 540 nm.

The difference in the distance dependence and amplification of upconverted emission introduced by proximal Au and Ag NPs are consistent with the optical properties of the different metal NPs measured experimentally. The longer optimal distance for enhancement observed in the case of Ag NPs is understood by considering their higher per volume extinction cross-section compared to Au NPs (Figure S3).[36] Extinction in metal NPs arises from both absorption and scattering processes. However, according to Mie theory, in small-diameter NPs, such as the 5 nm diameter NPs used in this work, the extinction coefficient is dominated by the absorption coefficient.[37] Therefore, Ag NPs have a larger absorption cross section at wavelengths resonant with the emission of the UCNPs compared to Au NPs of the same size. The optimal distance for radiation enhancement arises from a balance between quenching and metal-induced enhancement. The larger absorption cross-section of Ag NPs is consistent with the stronger quenching we observed (as seen in Figure 2 and Figure S3) and therefore the longer 10 nm optimal distance for radiation enhancement rather than the 5 nm distance found for Au NPs. While our simulations account for the size-corrected dielectric function measured by Johnson and Christy,[38,39] we expect, particularly for more sensitive Ag NPs, the dielectric function does not capture the size- and surface-dependent losses of the NPs.[40] The larger loss would give rise to a higher nonradiative rate for Ag NPs, consistent with the longer optimal distance of enhancement seen in experiment.

The quantum yield of UCNPs, or more generally of any flourophor, dramatically influences the magnitudes of the emission enhancement and the change in the decay rate they experience in proximity to metal NPs (Figure S4). We correlated the change in the measured decay times (Figure 6) with the measured upconversion enhancements (Figure 4) for these low quantum efficiency emitters. For example, for $NaYF_4$:Yb^{3+}, Er^{3+} UCNPs in the absence of metal NPs, the measured decay time τ is $1/(\Gamma_r + \Gamma_{nr}) = 298.2\ \mu s$ for the 540 nm emission peak, where Γ_r is the radiative decay rate and Γ_{nr} is the nonradiative decay rate due to intrinsic processes. The size-dependent quantum yield (QY) for similar UCNPs has previously been measured experimentally to be 10^{-3}.[9] From the measured lifetimes and reported $QY = \Gamma_r/(\Gamma_r + \Gamma_{nr})$, we estimate $\Gamma_r = 3.35\ s^{-1}$ and $\Gamma_{nr} = 3350\ s^{-1}$. In the presence of metal NPs, the greatest enhancement observed has been for the case of Ag NPs with a 10 nm oxide spacer layer where $\tau = 144.8\ \mu s$. Therefore the modified radiative rate (Γ_r') and nonradiative rate (Γ_{nr}') sum as $\Gamma_r' + \Gamma_{nr}' = 6906\ s^{-1}$. The partition between these rates depends on the

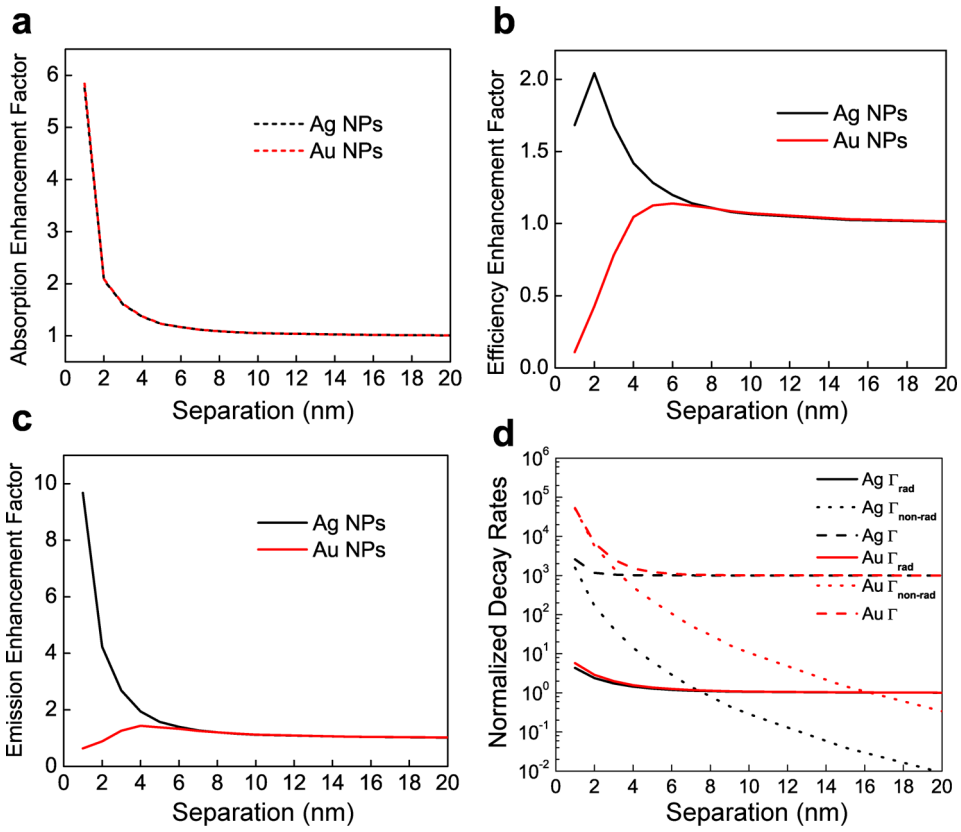

Figure 7. Electromagnetic simulations as a function of separation between Au or Ag NPs 6 nm in diameter and UCNPs with 0.1% quantum yield of the (a) absorption enhancement at the incident 980 nm excitation, (b) intrinsic emission efficiency of the UCNPs at 540 nm, (c) fluorescence enhancement in UCNPs at 540 nm, and (d) changes in the radiative, nonradiative, and total decay rates of the UCNPs in the presence of metal NPs (Note: the nonradiative decay rate arises from absorption in the metal, whereas the total decay rate includes intrinsic losses in the UCNPs).

increase in the Γ_{nr}' that arises from absorption in the metal NPs due to quenching as the UCNPs approach the metal NP arrays. Even if substantial quenching by the metal NPs were to occur, given the low quantum yield of these UCNPs, upconversion enhancement factors of ~30 are predicted, consistent with the enhancement measured experimentally and consistent with the measured changes in lifetime. This is unlike high quantum yield emitters, where quenching dominates the process and efficiency enhancement is small. The difference in the enhancement factors for 540 and 650 nm emission peaks in $NaYF_4$:Yb^{3+}, Er^{3+} UCNPs is consistent with wavelength-dependent nature of permittivity in Au and Ag NPs, which results in different absorption enhancement factors for the two emission peaks. Furthermore, since the quantum yield of the transition from the $F_{9/2}$ to $I_{15/2}$ (650 nm emission peak) is lower than the transition from the $S_{3/2}$ to $I_{15/2}$ (540 nm emission peak) by ~5.5 times, we can expect a larger plasmonic efficiency enhancement for the 650 nm peak (Figure S5).

CONCLUSIONS

In conclusion, we have studied metal-enhanced upconversion luminescence in a metal−oxide−UCNP trilayered structure where the thickness of the oxide spacer is precisely varied from 2 to 15 nm for four different metal−UNCP combinations. The luminescence enhancement is found to be strongly dependent upon the type of metal NPs. Time-resolved rise and decay time PL measurements show that the enhancement of upconverted luminescence arises from (1) nonresonant enhancement of the excitation pump at 980 nm by metal NPs, which enhances the absorption process in Yb^{3+} atoms and thereby increases the rate of energy transfer between lanthanide dopants during the two-photon upconversion process, and (2) plasmonic increase in the radiative rate of emission.

METHODS

Nanocrystal Synthesis. Colloidal UCNPs were synthesized according to our previous work.[25] The UCNPs were isolated through the addition of ethanol, centrifugation, and redispersion in hexane. Au[41] and Ag[42] NPs were synthesized according to previously reported methods.

Structure Fabrication. All samples were prepared on glass substrates that were cleaned with 2-propanol and blown dry with nitrogen. Au or Ag NP dispersions in octane were deposited by

spin-coating at 1000 rpm using a CEE200 spinner. The thickness of the metal NP layer was determined by atomic force microscopy (AFM) measurements to be ~35−40 nm. Al_2O_3 spacer layers, varying from 2 to 15 nm in thickness, were deposited using an ALD Cambridge Nanotech Savanna system at 150 °C. Spectroscopic ellipsometry measurements indicate a high percision control in oxide deposition (Figure S6). The precursors for the deposition process were water and trimethylaluminum. A monolayer of UCNP was then transferred on top of the oxide layer, as described below.

UCNP Monolayer Transfer. UCNP monolayers were formed using the interfacial assembly method as described previously.[25,29] A 1.5 × 1.5 × 1 cm^3 Teflon well was half-filled with ethylene glycol. One drop (~30 μL) of UCNP solution was spread onto the surface of the ethylene glycol subphase, and the well was quickly covered by a glass slide to lower the solvent (hexane) evaporation rate. The particle concentration of the UCNP solution was carefully adjusted until a large-area UCNP monolayer (covering >90% of surface area of the subphase) was obtained consistently. After 30 min, a glass substrate with an Al_2O_3-covered metal NP film was placed underneath the floating UCNP monolayer and was lifted upward to transfer the film, which was further dried under vacuum to remove residual ethylene glycol.

Structural and Optical Measurements. Transmission electron microscopy images were taken on a JEM-1400 microscope operating at 120 kV. Scanning electron microscopy was performed on a JEOL 7500F HRSEM operating at 2.0 kV. Atomic force microscopy images were acquired using a MFP-3D-BIO Asylum Research AFM operating in the tapping mode. Power X-ray diffraction patterns were obtained on a Rigaku Smartlab diffractometer at a scanning rate of 0.1° min^{-1} in the 2θ range from 10° to 90° (Cu Kα radiation, λ = 1.5418 Å). Optical absorption spectra were recorded using a Cary 5000 UV/Vis/NIR spectrophotometer. Upconversion luminescence was measured on a Fluorolog-3 spectrofluorometer (Jobin-Yvon) using excitation from a 980 nm diode laser with 1.06 W power and a 0.05 W/mm^2 power density. In lifetime measurments a biconvex lens with a 12.7 mm focal length was used to focus the light on the samples.

Simulations. The simulations were performed on a commercial finite-element-method-based solver (COMSOL Multiphysics) using a frequency domain solver. The structure was meshed using tetrahedral mesh elements with a 1 nm resolution inside the plasmonic spheres and a gradually increasing mesh size as we move away from the plasmonic structures with a maximum mesh element size of 50 nm. The simulation domain was surrounded by a perfectly matched layer to absorb the outward propagating radiation. The permittivity for the gold and silver was set using experimental data from the literature.[38,39] To calculate the absorption enhancement, the structure was illuminated with a plane wave at the pump wavelength, and the local field in the vicinity of the structure was simulated. The absorption enhancement is proprotional to the square of the field enhancement. The decay rates were simulated using the semiclassical approximation, which states that the decay rate for a two-level system at a given location is proportional to the power radiated by a dipole placed at the same location.[35]

Nanoimprint Patterning of Au NP Stripes. Au NP films were patterned in the form of stripes by nanoimprint lithography (NIL). To carry out the nanoimprting, 100 μL of a Au NP dispersion was dropped on a glass substrate. The glass substrate was quickly covered and pressed by a PDMS template, and the substrate and template were heated to 100 °C to cure the Au NP dispersion. After curing the solution for 1 min, the PDMS template was demolded from the glass substrate. After the NIL process, the Au NP stripe pattern was clearly and uniformly formed across the glass substrate over a 1.2 mm × 1.2 mm area. The Au NP stripe pattern was fabricated with a 2 μm width, 3 μm periodicity, and 100 nm height.

Spatially Resolved Photoluminescence Measurements. Spatially resolved measurements of the upconverted photoluminescence of patterned samples were measured under 976 nm illumination generated by a MIRA HP Ti:Sapphire laser pumped by an 18 W Verdi diode laser. The 976 nm light was focused to a 0.8 μm spot size through an Olympus BX2 modified microscope. Samples were mounted on a closed-loop piezo-controlled stage (Thorlabs Nanomax) and translated under the excitation. The mapping was conducted across an area of 20 μm by 20 μm with 0.4 μm step size. Luminescence was collected *via* a fiber and sent to a monochromator (iHR 550, Horiba) coupled to a Si CCD camera (Symphony, Horiba).

Photoluminescence Lifetime Measurements. A 1W, continuous wave, 980 nm laser light source was used. The excitation was modulated at 100 Hz with a Stanford Research Systems SR540 optical chopper, and the time-dependent luminescence was collected with the multichannel scaler unit integrated in the Fluorohub of a Jobin-Yvon Fluorolog-3 spectrofluorometer.

Conflict of Interest: The authors declare no competing financial interest.

Acknowledgment. We thank T. Gordon for assistance with ellipsometric measurements. M.S., X.Y., S.-H.H., U.K.C., N.E., C.B. M., and C.R.K. acknowledge support from the Office of Naval Research (ONR) Multidisciplinary University Research Initiative (MURI) on Optical Metamaterials through award N00014-10-1-0942. S.J.O., A.T.F., and C.R.K. acknowledge support from the U.S. Department of Energy, Office of Basic Energy Sciences, Division of Materials Science and Engineering, under Award No. DE-SC0002158. C.B.M. is also grateful to the Richard Perry University Professorship for support of his supervisor role.

Supporting Information Available: Luminescence spectra of $NaYF_4$:Yb, Er and $NaYF_4$:Yb, Tm UCNP monolayer film. Additional SEM images of UCNP monolayer. Comparison between absorption spectra of Ag NPs and Au NPs. Energy diagram of Er^{3+}, Yb^{3+}, and Tm^{3+}. Al_2O_3 ALD thickness characterized by spectroscopic ellipsometry. This material is available free of charge *via* the Internet at http://pubs.acs.org.

REFERENCES AND NOTES

1. Chatterjee, D. K.; Rufaihah, A. J.; Zhang, Y. Upconversion Fluorescence Imaging of Cells and Small Animals Using Lanthanide Doped Nanocrystals. *Biomaterials* **2008**, *29*, 937–943.
2. Shalav, A.; Richards, B. S.; Trupke, T.; Krämer, K. W.; Güdel, H. U. Application of $NaYF_4$:Er^{3+} Up-Converting Phosphors for Enhanced Near-Infrared Silicon Solar Cell Response. *Appl. Phys. Lett.* **2005**, *86*, 013505.
3. van der Ende, B. M.; Aarts, L.; Meijerink, A. Lanthanide Ions as Spectral Converters for Solar Cells. *Phys. Chem. Chem. Phys.* **2009**, *11*, 11081–11095.
4. Wang, H.-Q.; Batentschuk, M.; Osvet, A.; Pinna, L.; Brabec, C. J. Rare-Earth Ion Doped Up-Conversion Materials for Photovoltaic Applications. *Adv. Mater.* **2011**, *23*, 2675–2680.
5. Danger, T.; Koetke, J.; Brede, R.; Heumann, E.; Huber, G.; Chai, B. H. T. Spectroscopy and Green Upconversion Laser Emission of Er^{3+}-Doped Crystals at Room Temperature. *J. Appl. Phys.* **1994**, *76*, 1413–1422.
6. Rapaport, A.; Milliez, J.; Bass, M.; Fellow, L.; Cassanho, A. Review of the Properties of Up-Conversion Phosphors for New Emissive Displays. *J. Disp. Technol.* **2006**, *2*, 68–78.
7. Menyuk, N.; Dwight, K.; Pierce, J. W. $NaYF_4$: Yb,Er—An Efficient Upconversion Phosphor. *App. Phys. Lett.* **1972**, *21*, 159–161.
8. Wang, F.; Liu, X. Recent Advances in the Chemistry of Lanthanide-Doped Upconversion Nanocrystals. *Chem. Soc. Rev.* **2009**, *38*, 976–989.
9. Boyer, J.-C.; van Veggel, F. C. J. M. Absolute Quantum Yield Measurements of Colloidal $NaYF_4$: Er^{3+}, Yb^{3+} Upconverting Nanoparticles. *Nanoscale* **2010**, *2*, 1417–1419.
10. Sudheendra, L.; Ortalan, V.; Dey, S.; Browning, N. D.; Kennedy, I. M. Plasmonic Enhanced Emissions from Cubic $NaYF_4$:Yb: Er/Tm Nanophosphors. *Chem. Mater.* **2011**, *23*, 2987–2993.
11. Zhang, H.; Li, Y.; Ivanov, I. a; Qu, Y.; Huang, Y.; Duan, X. Plasmonic Modulation of the Upconversion Fluorescence in $NaYF_4$: Yb/Tm Hexaplate Nanocrystals Using Gold Nanoparticles or Nanoshells. *Angew. Chem., Int. Ed.* **2010**, *49*, 2865–2868.

12. Rai, V. K.; Menezes, L. D. S.; de Araújo, C. B.; Kassab, L. R. P.; da Silva, D. M.; Kobayashi, R. A. Surface-Plasmon-Enhanced Frequency Upconversion in Pr^{3+} Doped Tellurium-Oxide Glasses Containing Silver Nanoparticles. *J. Appl. Phys.* **2008**, *103*, 093526.
13. Paudel, H. P.; Zhong, L.; Bayat, K.; Baroughi, M. F.; Smith, S.; Lin, C.; Jiang, C.; Berry, M. T.; May, P. S. Enhancement of Near-Infrared-to-Visible Upconversion Luminescence Using Engineered Plasmonic Gold Surfaces. *J. Phys. Chem. C* **2011**, *115*, 19028–19036.
14. Anger, P.; Bharadwaj, P.; Novotny, L. Enhancement and Quenching of Single-Molecule Fluorescence. *Phys. Rev. Lett.* **2006**, *96*, 3–6.
15. Aslan, K.; Gryczynski, I.; Malicka, J.; Matveeva, E.; Lakowicz, J. R.; Geddes, C. D. Metal-Enhanced Fluorescence: An Emerging Tool in Biotechnology. *Curr. Opin. Biotechnol.* **2005**, *16*, 55–62.
16. Schietinger, S.; Aichele, T.; Wang, H.-Q.; Nann, T.; Benson, O. Plasmon-Enhanced Upconversion in Single $NaYF_4$:Yb^{3+}/Er^{3+} Codoped Nanocrystals. *Nano Lett.* **2010**, *10*, 134–138.
17. Lakowicz, J. R. Radiative Decay Engineering: Biophysical and Biomedical Applications. *Anal. Biochem.* **2001**, *298*, 1–24.
18. Goldys, E. M.; Drozdowicz-Tomsia, K.; Xie, F.; Shtoyko, T.; Matveeva, E.; Gryczynski, I.; Gryczynski, Z. Fluorescence Amplification by Electrochemically Deposited Silver Nanowires with Fractal Architecture. *J. Am. Chem. Soc.* **2007**, *129*, 12117–12122.
19. Parfenov, A.; Gryczynski, I.; Malicka, J.; Geddes, C. D.; Lakowicz, J. R. Enhanced Fluorescence from Fluorophores on Fractal Silver Surfaces. *J. Phys.Chem. B* **2003**, *107*, 8829–8833.
20. Szmacinski, H.; Lakowicz, J. R.; Catchmark, J. M.; Anderson, J. P.; Middendorf, L. Correlation Between Scattering Properties of Silver Particle Arrays and Fluorescence Enhancement. *Appl. Spectrosc.* **2009**, *62*, 733–738.
21. Pompa, P. P.; Martiradonna, L.; Torre, A. D.; Sala, F. D.; Manna, L.; De Vittorio, M.; Calabi, F.; Cingolani, R.; Rinaldi, R. Metal-Enhanced Fluorescence of Colloidal Nanocrystals with Nanoscale Control. *Nat. Nanotechnol.* **2006**, *1*, 126–130.
22. Ditlbacher, H.; Felidj, N.; Krenn, J. R.; Lamprecht, B.; Leitner, A.; Aussenegg, F. R. Electromagnetic Interaction of Fluorophores with Designed Two-Dimensional Silver Nanoparticle Arrays. *Appl. Phys. B: Laser Opt.* **2001**, *73*, 373–377.
23. Jensen, T. R.; Malinsky, M. D.; Haynes, C. L.; Van Duyne, R. P. Nanosphere Lithography: Tunable Localized Surface Plasmon Resonance Spectra of Silver Nanoparticles. *J. Phys. Chem. B* **2000**, *104*, 10549–10556.
24. Shimizu, K.; Woo, W.; Fisher, B.; Eisler, H.; Bawendi, M. Surface-Enhanced Emission from Single Semiconductor Nanocrystals. *Phys. Rev. Lett.* **2002**, *89*, 9–12.
25. Ye, X.; Collins, J. E.; Kang, Y.; Chen, J.; Chen, D. T. N.; Yodh, A. G.; Murray, C. B. Morphologically Controlled Synthesis of Colloidal Upconversion Nanophosphors and Their Shape-Directed Self-Assembly. *Proc. Natl. Acad. Sci. U. S. A.* **2010**, *107*, 22430–22435.
26. Wang, F.; Han, Y.; Lim, C. S.; Lu, Y.; Wang, J.; Xu, J.; Chen, H.; Zhang, C.; Hong, M.; Liu, X. Simultaneous Phase and Size Control of Upconversion Nanocrystals through Lanthanide Doping. *Nature* **2010**, *463*, 1061–1065.
27. Li, Z.; Zhang, Y. Monodisperse Silica-Coated Polyvinylpyrrolidone/$NaYF_4$ Nanocrystals with Multicolor Upconversion Fluorescence Emission. *Angew. Chem., Int. Ed.* **2006**, *118*, 7896–7899.
28. Yi, G. S.; Chow, G. M. Synthesis of Hexagonal-Phase $NaYF_4$:Yb,Er and $NaYF_4$:Yb,Tm Nanocrystals with Efficient Up-Conversion Fluorescence. *Adv. Funct. Mater.* **2006**, *16*, 2324–2329.
29. Dong, A.; Chen, J.; Vora, P. M.; Kikkawa, J. M.; Murray, C. B. Binary Nanocrystal Superlattice Membranes Self-Assembled at the Liquid-Air Interface. *Nature* **2010**, *466*, 474–477.
30. Agostino, S. D.; Sala, F. D. Active Role of Oxide Layers on the Nanostructures. *ACS Nano* **2010**, *4*, 4117–4125.
31. State, Y. *Proc. Am. Phys. Soc. Phys. Rev.* **1946**, *69*, 680.
32. Bykov, V. P. Spontaneous Emission from a Medium with a Band Spectrum. *Sov. J. Quant. Electron.* **1975**, *4*, 861–871.
33. Yablonovitch, E. Inhibited Spontanous Emission in Solid-State Physics and Electroonics. *Phys. Rev. Lett.* **1987**, *58*, 2059–2062.
34. Pisarska, J. O.; Ryba-romanowski, W. I.; Dominiak-dzik, G. R. Energy Transfer from Yb to X (X = Tm, Er) in Lead Borate Glasses. *J. Mol. Struct.* **2005**, *XXXV*), 837–842.
35. Novotny, L.; Hecht, B. *Principles of Nano-Optics*; Cambridge University Press, 2006.
36. Amendola, V.; Bakr, O. M.; Stellacci, F. A Study of the Surface Plasmon Resonance of Silver Nanoparticles by the Discrete Dipole Approximation Method: Effect of Shape, Size, Structure, and Assembly. *Plasmonics* **2010**, *5*, 85–97.
37. Liu, X.; Atwater, M.; Wang, J.; Huo, Q. Extinction Coefficient of Gold Nanoparticles with Different Sizes and Different Capping Ligands. *Colloid Surf. B* **2007**, *58*, 3–7.
38. Johnson, P. B.; Christy, R. W. Optical Constant of the Noble Metals. *Phys. Rev. B* **1972**, *6*, 4370–4379.
39. Zhou, H. S.; Honma, I.; Komiyama, H.; Haus, J. W. Controlled Synthesis and Quantum-Size Effects in Gold-Coated Nanoparticles H. S. *Phys. Rev. B* **1994**, *50*, 52–57.
40. Drachev, V. P.; Chettiar, U. K.; Kildishev, A. V.; Yuan, H.-K.; Cai, W.; Shalaev, V. M. The Ag Dielectric Function in Plasmonic Metamaterials. *Opt. Express* **2008**, *16*, 1186–1195.
41. Ye, X.; Chen, J.; Murray, C. B. Polymorphism in Self-Assembled AB_6 Binary Nanocrystal Superlattices. *J. Am. Chem. Soc.* **2011**, *133*, 2613–20.
42. Yin, Y.; Erdonmez, C.; Aloni, S.; Alivisatos, A. P. Faceting of Nanocrystals during Chemical Transformation: from Solid Silver Spheres to Hollow Gold Octahedra. *J. Am. Chem. Soc.* **2006**, *128*, 12671–12673.